Pergamon

Scripta Materialia, Vol. 38, No. 2, pp. 245–251, 1998
Elsevier Science Ltd

1359-6462/98 $19.00 + .00

PII S1359-6462(97)00433-8

FATIGUE-CRACK GROWTH OF SMALL CRACKS IN A DIRECTIONALLY-SOLIDIFIED NICKEL ALUMINIDE WITH MOLYBDENUM ADDITIONS

Moon-Hee Hong*, J.M. McNaney, and R.O. Ritchie
Department of Materials Science and Mineral Engineering, University of California, Berkeley, CA 94720-1760

(Received August 12, 1997)
(Accepted September 10, 1997)

Introduction

In recent years, aluminide intermetallic compounds, such as NiAl and TiAl, have been contemplated for potential high-temperature structural use in aero-engine applications as possible replacement for the nickel-base superalloys. NiAl, for example, has a relatively low density (5.95 g/cm^3) approximately two-thirds that of superalloys, extremely high oxidation resistance and high thermal conductivity (1). However, like many intermetallics, its application is severely compromised by its very low ductility and toughness properties at ambient temperatures; moreover, NiAl displays lower strength at elevated temperatures. Accordingly, much alloy design and microstructure research on NiAl has been focused on attempts to improve the low-temperature ductility, fracture toughness and high-temperature strength of this intermetallic (2–7).

One promising approach has been through the use of *in situ* composite reinforcement, specifically by directional solidification of two-phase NiAl eutectic microstructures, obtained from ternary alloying additions of refractory metals (6,7). For instance, it has been reported (6,7) that aligned-eutectic composites of NiAl-Cr, NiAl-V, and NiAl-Mo show significantly higher fracture toughness than NiAl; compared to a K_{Ic} of ~6 MPa$\sqrt{m}$ for polycrystalline NiAl (4), the aligned eutectics display resistance-curve behavior with steady-state toughness values up to ~30 MPa$\sqrt{m}$. Such ductile-phase toughening has been attributed to crack bridging and subsequent plastic deformation of the eutectic phase, i.e., to crack-tip shielding mechanisms which act primarily in the wake of the crack tip.

However, despite such progress in the toughening of NiAl-based materials under monotonic loading, nothing is known about their fatigue-crack growth properties under cyclic loads. This is important since it is known from studies on other ductile-phase toughened intermetallics (γ-TiAl, Nb_3Al, $MoSi_2$) that extrinsic toughening (crack-tip shielding) mechanisms such as crack bridging are far less potent, and indeed degrade substantially, under cyclic loading due to premature fatigue failure of the ductile phase (8–11). Moreover, for many engine applications such as turbine blades, it is the fatigue properties of small flaws (typically below ~500 μm in size), especially at near-threshold stress intensities, that are limiting with respect to lifetime considerations. Again, with small cracks, the beneficial effects of the

Work supported by the U.S. Air Force Office of Scientific Research under a subcontract from the University Research Initiative Grant No. F49620-93-1-0289 to the University of Michigan, Ann Arbor.
*On leave from the Agency for Defense Development, Taejon, Korea.

shielding mechanisms such as crack bridging are muted due to the difficulty in developing an equilibrium bridging zone with cracks of restricted wake (e.g., 12,13).

Accordingly, it is the objective of the current note to present the first results on the fatigue behavior of NiAl aligned-eutectic composites. Specifically the near-threshold fatigue-crack propagation properties of physically-small (<400 μm) surface cracks† in one such alloy, namely a DS NiAl-9Mo (at.%), are examined as a function of the load ratio, with the objective of discerning the salient mechanisms affecting crack-growth behavior.

Materials and Experimental Procedures

The DS NiAl-9at%Mo *in situ* composite was processed using directional solidification techniques at the University of Michigan, Ann Arbor. Specifically, elemental Ni, Al and Mo were arc-melted into "buttons" in a crucible under a static argon atmosphere; the buttons were turned over and re-melted several times to insure appropriate mixing. The arc-melted buttons were subsequently crushed to powder and placed in an alumina crucible in an evacuated ($<0.6 \times 10^{-6}$ torr) furnace chamber; the chamber was then back-filled with a slight positive pressure of flowing argon and the furnace heated to 1550°C for 30 min. Directional solidification was then achieved by lowering the crucible into the cool zone of the furnace at a rate of 8.9 mm/hr. Ingot sizes were approximately 100 mm long with a ~20 mm diameter. Full details of the processing are given elsewhere (14).

The resulting cellular eutectic microstructure consisted of a NiAl phase in the form of ~100–200 μm diameter "islands", within the NiAl-Mo eutectic, the latter containing Mo rods, approximately 5–15 μm in length with a 1–2 μm diameter, aligned nominally parallel to the solidification direction. The Mo rod alignment was changed radically near the cellular NiAl regions where it decorated the cell boundaries; in addition, the distribution of these cells was not uniform within the ingot. Interstitial contents were typical of commercial purity NiAl, namely 0.0047 wt.% C, 0.003 wt.% O, <0.0005 wt.% N, and 0.0013 wt.% S (14).

Fatigue-crack propagation rates for a small (<400 μm) surface cracks were measured by observing the top (tension) surface of cantilever-bend specimens (2 mm square, 70 mm in length) cycled at a sinusoidal frequency of 25 Hz in a constant-displacement testing machine (Fatigue Dynamics SS40 variable-speed testing machine). Samples were machined in the longitudinal (L) orientation with crack growth perpendicular to the solidification direction. Tension surfaces were polished to a finish of ~1 μm prior to testing. Small cracks were then initiated from electro-discharge machining (EDM) pits, generated at high current (8 A) and placed along the longitudinal axes of the top surface. On cyclic loading, the pre-cracks were allowed to extend beyond the EDM heat-affected zone before data acquisition was commenced.

Specimens were cycled at three different load ratios (ratio of minimum to maximum loads) of $R = -0.3$, 0 and 0.35, in room temperature air. Tests were periodically interrupted by removing the specimen for optical examination; samples were examined after the first cycle to determine any crack extension during initial loading and then subsequently after 10^2 to 10^4 cycle intervals until failure. Average growth rates were evaluated from the amount of crack extension between two discrete measurement intervals. Stress-intensity factors were computed from the Newman-Raju linear-elastic solutions for a semi-elliptical surface crack in bending (15). A crack depth to half surface crack length ratio of $a/c = 0.78$ was used, based on fractographic examination of several samples broken open during the fatigue testing. Further details of these experimental procedures for small-crack testing in brittle

†Although physically small in size, such cracks are large compared to the characteristic microstructural dimensions in this alloy.

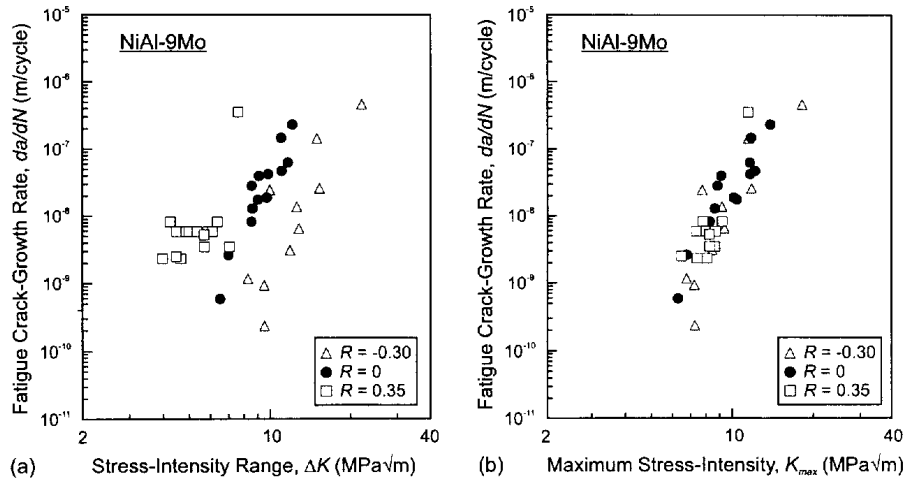

Figure 1. Variation in ambient-temperature fatigue crack-growth rates, *da/dN*, with applied load ratio R for small surface cracks ($c < 400$ μm) in a directionally solidified DS NiAl-9Mo *in situ* composite, with data plotted as a function of the applied (a) stress-intensity range, ΔK, and (b) maximum stress intensity (K_{max}).

materials have been presented elsewhere (16). Following fatigue testing, all fracture surfaces were imaged optically and in the scanning electron microscope (SEM).

Results and Discussion

Results showing the variation in fatigue-crack growth rates, *da/dN*, of small surface cracks ($c < 400$ μm) in the DS NiAl-9Mo *in situ* composite, at load ratios of -0.3, 0 and 0.35, are plotted in Figure 1 as a function of the applied alternating, ΔK, and maximum, K_{max}, stress intensities; data are shown primarily for the near-threshold regime, over the range $\sim 10^{-10}$ to 10^{-6} m/cycle. Akin to most low ductility materials (e.g., 11,16,17), growth rates show a strong dependency on K, and are increased at a given ΔK value with increasing R (Fig. 1a). However, this load-ratio effect can be essentially normalized by plotting growth rates in terms of K_{max} (Fig. 1b); indeed, in terms of K_{max}, for the range of load ratios studied there appears to be a R-independent fatigue threshold (below which no appreciable crack extension is apparent) of $K_{max,TH} \sim 6$ MPa$\sqrt{m}$. This compares to an average fracture toughness of $K_{Ic} = 16.2$ MPa$\sqrt{m}$ measured‡ for this material in this orientation (18). Such behavior implies that near-threshold cyclic crack growth in this material is primarily controlled by K_{max}, similar to behavior in most (non-transforming) ceramics (16,17) and the more brittle intermetallics (11).

The morphology of such small-crack growth, specifically under tension-tension ($R \sim 0$) cycling, is shown in Fig. 2, where crack extension occurred in stable fashion, from a initial crack length of $c \sim 80$ to a final length of ~ 450 μm, along a direction perpendicular to the applied stress (indicated by arrow). Scanning electron microscopy of the crack path, however, revealed differing trajectories depending upon the local orientation of the Mo rods with respect to the direction of loading. In regions where the crack encounters rounded Mo particles (where the rod axis is presumably aligned parallel to the crack front), the particles remain unbroken and extensive crack deflection occurs as the crack tends to circumvent the periphery of the eutectic particles (Fig. 3a), consistent with considerations of the modulus mismatch between the particle and matrix (19,20). Conversely, where the axis of the rods is

‡Valid measurements (18) were made using fatigue-precracked compact-tension samples, in accordance with ASTM E399 standards.

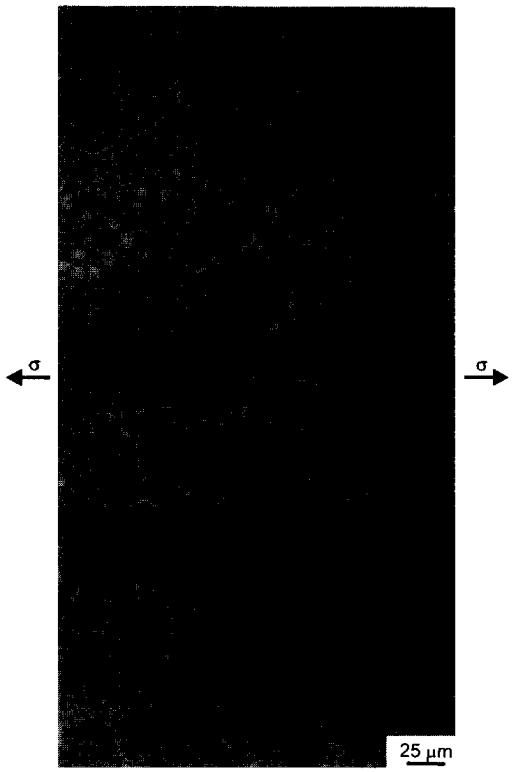

Figure 2. Optical micrograph of small fatigue crack growth in DS Ni-Al-9Mo, showing stable cracking along a direction perpendicular to the applied loading (indicated by arrows). The white irregular particles are the Mo rods.

oriented nominally perpendicular to the crack plane, the crack bisects the rods causing their failure (Fig. 3b).

No evidence of crack bridging by intact Mo-particle ligaments could be detected under cyclic loading conditions; indeed all the Mo-particles that intersected the crack path were found to be either broken or circumvented (Fig. 4). This is marked contrast to behavior under monotonic loading where extensive crack bridging by the eutectic phase has been reported to be responsible for the significant resistance-curve toughening (5–7). As noted above, cyclic loading invariably results in the premature failure of the metallic particles, simply because cyclic plastic strain and resulting fatigue damage can be more readily accumulated in the ductile phase. In fact, such behavior has been observed in several ductile-phase toughened, brittle-matrix composites, including TiNb- and Nb-reinforced γ-TiAl (8,9), and Nb-reinforced Nb_3Al (10) and $MoSi_2$ (11). The failure of the eutectic phase, however, does induce a somewhat rougher fracture-surface morphology, which may promote alternative shielding mechanisms, i.e., crack closure, under cyclic loading. This can be seen in Figure 4 where asperity-to-asperity contact is clearly apparent between the mating crack surfaces.

Regression fits to the crack-growth rate data in Figure 1 confirm the marked dependency on stress intensity. In terms of the simple Paris power-law relationship ($da/dN \propto \Delta K^m$), growth rates are an approximate function of ΔK^7; however, this relationship masks the true dependency on K_{max}. An improved approach is to express the data in terms of a modified Paris-law relation to include the effects of both ΔK and K_{max} (16,21); using this scheme, the growth-rate relationship for the NiAl-9Mo composite was found to be approximately $da/dN \propto (K_{max})^6(\Delta K)^1$, which confirms the dominant role of K_{max}. Through comparison to behavior in other ductile and brittle material systems (17), we conclude that the K_{max}-dependence results from crack advance primarily by static fracture of the brittle NiAl and

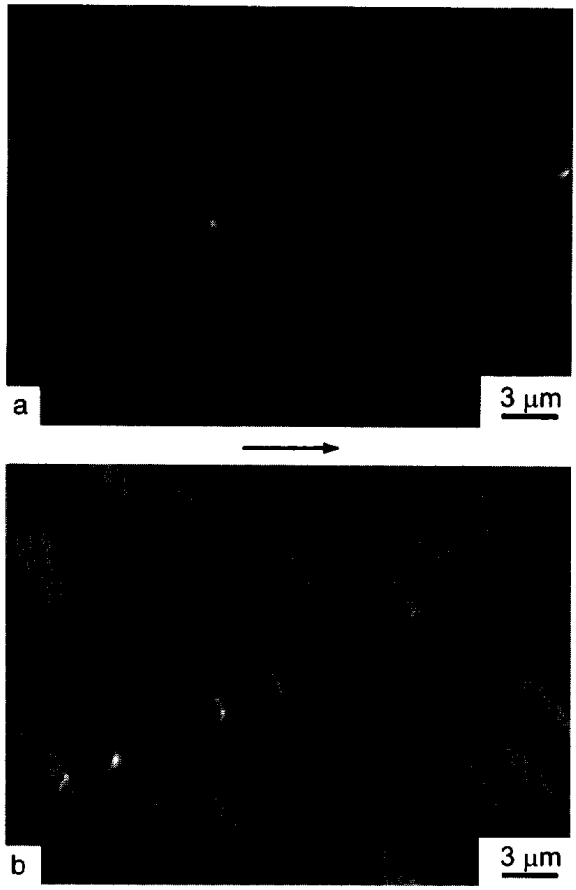

Figure 3. Scanning electron micrographs of the trajectory of small fatigue cracks under $R \sim 0$ loading in DS NiAl-9Mo, showing crack/Mo particle interactions; specifically, the crack path tends (a) to circumvent the periphery of the rounded Mo particles, and (b) to bisect the aligned Mo particles. Arrow indicates general direction of crack growth.

NiAl-Mo eutectic phases (and possibly from a limitation in crack closure at high R), whereas the minimal ΔK-dependence results from intrinsic fatigue failure of the Mo phase and the consequent cyclic-loading induced suppression of crack bridging behind the crack tip.

Conclusions

Based on a study of the near-threshold fatigue-crack growth behavior of small surface cracks (80 μm $\leq$ $c \leq$ 450 μm) in a directionally-solidified NiAl-9at.%Mo *in situ* composite at ambient temperatures, the following conclusions can be made:

1. Rates of fatigue-crack growth in the DS NiAl-9Mo are found to be strongly dependent upon the maximum stress intensity and more weakly dependent upon the stress-intensity range, specifically $da/dN \propto (K_{max})^6(\Delta K)^1$ over the range $\sim 10^{-10}$ to 10^{-6} m/cycle ($-0.3 \leq R \leq 0.35$). Thus, in terms of ΔK, growth rates increase with increasing load ratio, yet the R-ratio dependence can be normalized by characterizing in terms of K_{max}. Over the range of load ratios examined, there appears to be a R-independent fatigue threshold of $K_{max,TH} \sim 6$ MPa$\sqrt{m}$ ($\sim$ 37% of K_{Ic}).
2. The interaction of the small fatigue cracks with the Mo eutectic rods was dependent upon the orientation of the rods with respect to the loading direction. In regions where the rod axis was aligned

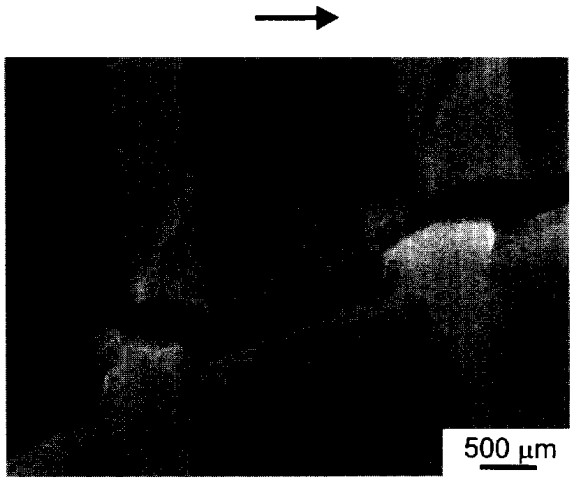

Figure 4. Higher magnification scanning electron micrograph of crack/Mo particle interactions during cyclic fatigue-crack growth in DS NiAl-9Mo at $R \sim 0$, showing the failure of the Mo particles in the wake of the crack tip. Arrow indicates general direction of crack growth.

nominally parallel to the crack front, the Mo particles remained unbroken and the crack merely circumvented the particles; conversely, where the axis of the rods was aligned nominally perpendicular to the crack plane, interception with the fatigue crack resulted in their fracture.

3. Unlike reported behavior under monotonic loading where crack bridging by unbroken Mo rods acts to promote resistance-curve toughness, absolutely no evidence of such crack bridging could be detected under cyclic loading; all Mo-particles that intersected the crack path were either broken or circumvented.
4. It is concluded that for the DS NiAl-9Mo *in situ* composite in the small crack/near-threshold regime studied, the mechanisms of fatigue-crack growth involve a K_{max}-controlled crack-advance mechanism in the NiAl and NiAl-Mo eutectic phases and a ΔK-controlled suppression of crack bridging, the latter resulting from fatigue failure of the Mo eutectic rods.

Acknowledgments

This work was supported by the U.S. Air Force Office of Scientific Research under the University Research Initiative Grant No. F49620-93-1-0289 to the University of Michigan, Ann Arbor. Thanks are due to Prof. Ron Gibala and Matt Kush for processing the NiAl-Mo alloy and to Dr. K. T. Venkateswara Rao for many helpful discussions.

References

1. R. Darolia, J. Metal. 43, 44 (1991).
2. P. R. Subramanian, M. G. Mendiratta, D. B. Miracle, and D. M. Dimiduk, in Intermetallic Matrix Composites, Symp. Vol. 194, p. 147, Materials Research Society, Pittsburgh, PA (1990).
3. R. Darolia, D. Lahrman, and R. Field, Scripta Metall. Mater. 26, 1007 (1992).
4. K. S. Kumar, S. K. Mannan, and R. K. Viswanadham, Acta Metall. Mater. 40, 1201 (1992).
5. D. R. Johnson, X. F. Chen, B. F. Oliver, R. D. Noebe, and J. D. Whittenberger, Intermetallics. 3, 141 (1995).
6. F. E. Heredia, M. Y. He, G. E. Lucas, A. G. Evans, H. E. Dève, and D. Konitzer, Acta Metall. Mater. 14, 505 (1993).
7. S. M. Joslin, X. F. Chen, B. F. Oliver, and R. D. Noebe, Mater. Sci. Eng. A196, 9 (1995).
8. K. T. Venkateswara Rao, G. R. Odette, and R. O. Ritchie, Acta Metall. Mater. 40, 353 (1992).

9. K. T. Venkateswara Rao, G. R. Odette, and R. O. Ritchie, Acta Metall. Mater. 42, 893 (1994).
10. L. Murugesh, K. T. Venkateswara Rao, and R. O. Ritchie, Scripta Metall. Mater. 29, 1107 (1993).
11. K. Bardrinarayanan, A. L. McKelvey, K. T. Venkateswara Rao, and R. O. Ritchie, Metall. Mater. Trans. A. 27A, 3781 (1996).
12. S. Suresh and R. O. Ritchie, Int. Metals Rev. 29, 445 (1984).
13. R. O. Ritchie and J. Lankford, Mater. Sci. Eng. A84, 11 (1986).
14. A. Misra, Z. L. Wu, M. T. Kush, and R. Gibala, Mater. Sci. Eng. in press (1997).
15. J. C. Newman, Jr. and I. S. Raju, Eng. Fract. Mech. 15, 185 (1981).
16. R. H. Dauskardt, M. R. James, J. R. Porter, and R. O. Ritchie, J. Am. Ceram. Soc. 75, 759 (1992).
17. R. O. Ritchie and K. T. Venkateswara Rao, in ECF-11-Mechanisms and Mechanics of Damage and Failure, Proc. 11th European Conf. on Fracture, ed. J. Petit, Vol. 1, p. 53, EMAS, Warley, UK (1996).
18. M.-H. Hong, J. M. McNaney, and R. O. Ritchie, Metall. Mater. Trans. A. in review (1997).
19. R. W. Davidge and T. J. Green, J. Mater. Sci. 3, 629 (1968).
20. R. O. Ritchie, R. M. Cannon, B. J. Dalgleish, R. H. Dauskardt, and J. M. McNaney, Mater. Sci. Eng. A166, 221 (1993).
21. S.-Y. Liu and I.-W. Chen, J. Am. Ceram. Soc. 74, 1197 (1991).